11458 *Biochemistry* **2009,** *48,* 11458–11469
DOI: 10.1021/bi901196x

BIOCHEMISTRY
including biophysical chemistry & molecular biology
Article

The Role of Key Amino Acids in the Photoactivation Pathway of the *Synechocystis* Slr1694 BLUF Domain[†]

Cosimo Bonetti,[‡] Manuela Stierl,[§] Tilo Mathes,[§] Ivo H. M. van Stokkum,[‡] Katharine M. Mullen,[‡] Thomas A. Cohen-Stuart,[‡] Rienk van Grondelle,[‡] Peter Hegemann,[§] and John T. M. Kennis*[,‡]

[‡]*Biophysics Group, Department of Physics and Astronomy, Faculty of Sciences, VU University, De Boelelaan 1081, 1081 HV, Amsterdam, The Netherlands and* [§]*Institut für Biologie/Experimentelle Biophysik, Humboldt Universität zu Berlin, Invalidenstrasse 42, D-10115 Berlin, Germany*

Received July 14, 2009; Revised Manuscript Received October 22, 2009

ABSTRACT: BLUF (blue light sensing using FAD) domains belong to a novel group of blue light sensing receptor proteins found in microorganisms. We have assessed the role of specific aromatic and polar residues in the *Synechocystis* Slr1694 BLUF protein by investigating site-directed mutants with substitutions Y8W, W91F, and S28A. The W91F and S28A mutants formed the red-shifted signaling state upon blue light illumination, whereas in the Y8W mutant, signaling state formation was abolished. The W91F mutant shows photoactivation dynamics that involve the successive formation of FAD anionic and neutral semiquinone radicals on a picosecond time scale, followed by radical pair recombination to result in the long-lived signaling state in less than 100 ps. The photoactivation dynamics and quantum yield of signaling state formation were essentially identical to those of wild type, which indicates that only one significant light-driven electron transfer pathway is available in Slr1694, involving electron transfer from Y8 to FAD without notable contribution of W91. In the S28A mutant, the photoactivation dynamics and quantum yield of signaling state formation as well as dark recovery were essentially the same as in wild type. Thus, S28 does not play an essential role in the initial hydrogen bond switching reaction in Slr1694 beyond an influence on the absorption spectrum. In the Y8W mutant, two deactivation branches upon excitation were identified: the first involves a neutral semiquinone $FADH^{\bullet}$ that was formed in ~1 ps and recombines in 10 ps and is tentatively assigned to a $FADH^{\bullet}-W8^{\bullet}$ radical pair. The second deactivation branch forms $FADH^{\bullet}$ in 8 ps and evolves to $FAD^{\bullet-}$ in 200 ps, which recombines to the ground state in about 4 ns. In the latter branch, W8 is tentatively assigned as the FAD redox partner as well. Overall, the results are consistent with a photoactivation mechanism for BLUF domains where signaling state formation proceeds via light-driven electron and proton transfer from Y8 to FAD, followed by a hydrogen bond rearrangement and radical pair recombination.

Blue light photoreceptors using flavin cofactors have been the focus of recent research because of their novel mechanisms of photoactivation in contrast to "classical" photoreceptors like phytochromes and rhodopsins. Especially members of the BLUF[1] (blue light photoreceptors using FAD) family (*1*−*3*) show an especially intriguing light-induced proton network rearrangement resulting in a 10−15 nm red-shifted spectrum of the signaling state. The BLUF domain shows a ferredoxin-like fold consisting of a five-stranded β-sheet with two α-helices packed on one side of the sheet, with the isoalloxazine ring of flavin adenine dinucleotide (FAD) positioned between the two α-helices (*4*−*12*). FAD is noncovalently bound to the protein through a number of hydrogen bonds and hydrophobic interactions. Figure 1 shows the three-dimensional structure of the *Synechocystis* Slr1694 BLUF domain (also known as PixD) in its proposed dark and light states, with the FAD binding pocket highlighted (*7*). Conserved tyrosine (Y8), glutamine (Q50), and asparagine (N32) side chains are involved in an intricate hydrogen bond network with flavin. The molecular identities of the BLUF dark and photoactivated states remain controversial as X-ray and NMR structures have given different orientations for the conserved glutamine in the dark (i.e., with the amino group hydrogen bonded to the conserved tyrosine or to FAD C_4=O; see Figure 1A,B). A similar issue holds for W91 and M93, which were found either close to FAD or exposed to the solvent (*4*−*8*, *12*, *13*).

The current opinion on the photoactivation of the BLUF domains as observed by steady-state FTIR (*14*−*16*), Raman (*17*, *18*), ultrafast visible and IR spectroscopy (*19*−*25*), and quantum-chemical calculations (*26*−*29*) includes light-induced radical pair formation by electron and proton transfer from an essential tyrosine side chain (Y8) to the flavin cofactor on the picosecond time scale. Subsequently, hydrogen bond rearrangement takes place, possibly involving ~180° rotation of the amide group of an essential glutamine side chain (Q50) which is followed by radical

[†]This work was supported by the European Union through the LaserLab Europe Access Programme (M.S., T.M., and P.H.). C.B. was supported by the Life Sciences Council of The Netherlands Organization for Scientific Research (NWO-ALW). K.M.M. by was supported by Computational Science Grant 635.000.014 from NWO. J. T.M.K. was supported by NWO-ALW through a VIDI fellowship. Funding for the laser equipment was provided by NWO-ALW through investment grant 834.05.001

*Corresponding author: e-mail, john@nat.vu.nl; phone, +31205-987212; fax, +31205987999.

[1]Abbreviations: FAD, flavin adenine dinucleotide; BLUF, blue light sensing using FAD; EADS, evolution-associated difference spectrum; SADS, species-associated difference spectrum; FTIR, Fourier-transform infrared; IRF, instrument response function.

 Published on Web 10/28/2009

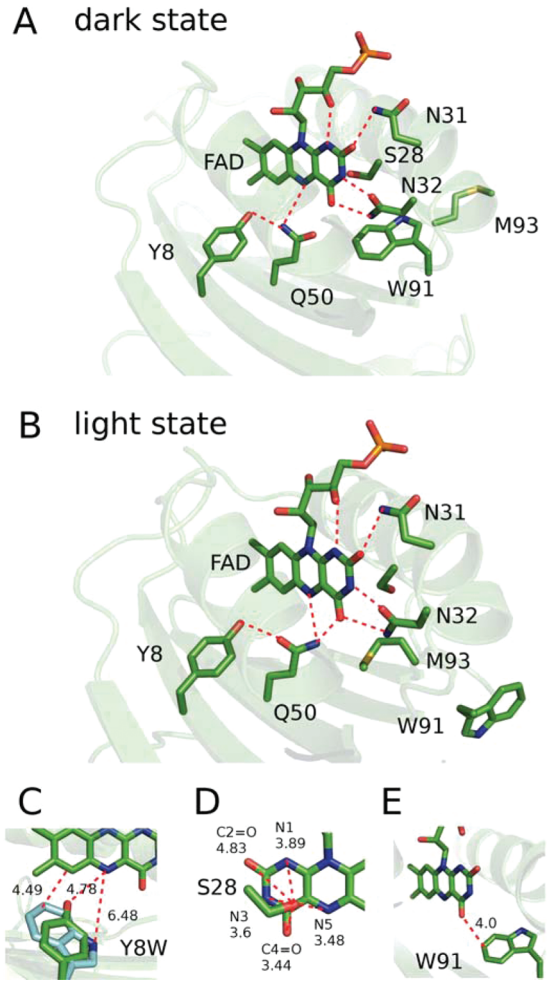

FIGURE 1: Three-dimensional structure of the *Synechocystis* Slr1694 BLUF domain in its proposed dark (A) and light (B) states. Conserved tyrosine (Y8), glutamine (Q50), and asparagine (N32) side chains are involved in an intricate hydrogen bond network with flavin. The interactions of the here investigated key amino acids with the flavin in the dark state are displayed in (C), (D), and (E). The numbers refer to the corresponding distances (Å) in the crystal structure.

pair recombination in less than 100 ps. The resulting reoxidized flavin forms a hydrogen bond switched network in the flavin binding pocket.

Although Y8 has been experimentally shown to be essential for electron transfer, it is not certain whether the proton is also transferred from this residue. Also, the mode of signal transduction in BLUF domains remains largely unclear since structural changes are mainly limited to the side chains in the immediate vicinity of FAD. A possibly light-induced displacement of the semiconserved W104 in AppA by the conserved M106 and the concomitant backbone rearrangement is a possible candidate for signal transduction as implicated by crystal structures (*6*, *7*, *30*), NMR spectroscopy (*10*, *11*), FTIR spectroscopy (*30*), and physiological observations (*31*). The backbone rearrangement might affect the oligomerization state of a recently proposed oligomeric BLUF/effector complex and thereby transduce the biological signal (*32*).

One major problem in understanding the nature of the primary intermediates is the conformational heterogeneity of the ground state in BLUF domains (*9*, *20*) which leads to a complicated transient behavior after light excitation (*21*). The data recorded by ultrafast spectroscopy therefore has to be analyzed by modeling the reaction using a procedure called target analysis (*33*). To simplify the analysis, it would be feasible to stabilize the intermediates so they can be studied under steady-state(-like) conditions. Another aspect in the study of BLUF photoreceptors is their rather large variety in their transient behavior. Despite their high sequence homology the signaling state lifetime of BLUF domains varies from Slr1694, BlrB (*5*), and *Thermosynechococcus* TePixD (*34*) with around 10 s to AppA (*35*) and YcgF (*36*) with 50−100-fold slower decay times.

In the AppA BLUF domain it was shown that the semiconserved tryptophan in the vicinity of FAD (W104) also contributes to electron transfer to the flavin (*20*, *37*). The latter observation lended support to the "W-in" conformation of W104 in dark-state AppA. Tryptophan at this position is conserved in 85% of the BLUF domain family.

One interesting candidate which might explain the diverse behavior in BLUF domains might be S28 in Slr1694. Serine is conserved at this position in 43% of the BLUF domain family. S28 is a polar, acidic residue in close vicinity to FAD. The hydroxyl group of this serine introduces a dipolar interaction with the heteroatoms of the flavin and therefore alters the spectroscopic properties of the protein and possibly also the dynamics after light excitation. Recent quantum mechanical studies on AppA proposed an essential role of this residue (S41) for the theoretical description of the red-shifted spectrum of the light-activated state (*38*). Moreover, in the calculations, S41 was found to switch conformation in concert with W104 upon light absorption. It is thus of interest to study the photodynamics of the S28A mutant of Slr1694.

It was shown previously that the conserved tyrosine (Y8 in Slr1694, Y21 in AppA) is essential for BLUF photoactivation by acting as the electron donor and hydrogen bond donor/acceptor of the conserved glutamine (*20*, *22*−*24*, *34*, *39*−*41*). It is known that, besides tyrosine, tryptophan can act as an efficient electron donor to flavin. For AppA, removal of Y21 by site-directed mutagenesis leads to redundant electron transfer processes from W104 which result in short-lived FAD-W radical pairs but not in a stable photoproduct (*20*, *23*). The question then arises whether W can take up some of the roles of the conserved Y in BLUF domains, i.e., electron transfer and hydrogen bond switch capabilities. For this reason we constructed the Y8W mutant of Slr1694. In this work we studied the role of these (semi)conserved amino acid side chains in the vicinity of the flavin in Slr1694 by ultrafast visible spectroscopy on mutated proteins with respect to their role in electron/proton transfer during the primary processes.

MATERIALS AND METHODS

Sample Preparation. Mutations were introduced into pET28a(+)-slr1694 (*19*, *42*) by site-directed mutagenesis (QuikChange; Stratagene) using the primers in Table 1. The mutated DNA was confirmed by sequence analysis. Proteins were expressed in *Escherichia coli* strain BL21(DE3)pLysS overnight at 18 °C in the presence of 0.7 mM IPTG and purified as described before (*22*).

Experimental System. Time-resolved measurements on the Slr1694 mutants presented in this paper were performed on a visible pump−visible probe setup. The system uses a Coherent Legend-USP Ti:Sapphire amplifier oscillator (1 kHz), providing a light source with a central wavelength of 800 nm, bandwidth of 30 nm at full-width half-maximum, with an energy of 2.5 mJ/pulse and

Table 1: Oligonucleotides Used for Site-Directed Mutagenesis[a]

oligonucleotide	sequence (5′ → 3′)
Y8W_fw	GTTTGTACCGTTTGATTT**GG**AGCAGTCAGGGCATTCCC
Y8W_rv	GGGAATGCCCTGACTGCT**CC**AAATCAAACGGTACAAAC
Slr_S28A_fw	GATATCTTAGAATCT**G**CCCAAAGAAATAATCCGGC
Slr_S28A_rv	GCCGGATTATTTCTTTGGG**C**AGATTCTAAGATATC
Slr_W90F_fw	GAAGAAACTTCGAGGTTT**TC**TCTATGCAAGCGATC
Slr_W90F_rv	GATCGCTTGCATAGA**GA**AAACCTCGAAGTTTCTTC

[a]The mismatched bases are printed in bold.

a duration of ~40 fs. The 800 nm pulse is split in two parts: one part is frequency-doubled in a BBO crystal to generate a 400 nm pump beam which triggers the photoreaction; the remaining fraction of the fundamental 800 nm beam is focused on a rotating CaF_2 crystal to generate a white light continuum that is used to probe the sample. The polarization between pump and probe beams was set to the magic angle (54.7°). The probe pulse is focused on the sample by parabolic mirrors to avoid chromatic aberration, for the same reason an achromatic lens (fl: 200 mm) is used to focus the pump. The pump pulse is progressively delayed with respect to the probe using a 60 cm long delay stage (Newport IMS-6000) to cover a time window up to 3.7 ns. The sample, placed in a quartz flow cell of 2 mm optical path, is fixed in the focus plane of the two focusing elements (achromatic lens and parabolic mirror) and circulated by a peristaltic pump. Behind the sample, the pump and probe beams are spatially separated; only the probe beam is collimated and focused on the entrance slit of a spectrograph (Oriel) and by spectrally dispersed across a home-built camera equipped with a 256 element photodiode array (Hamamatsu). This 256 pixel array is read out, and the data were parsed to a computer calculating the transient absorption. Out of the thousand pulses per second, 500 pump pulses are blocked to allow to measure the difference in absorption of the white light between molecules pumped and nonpumped. The transient absorption setup was described in detail in ref *43*.

Data Analysis. The time-resolved data can be described in terms of a parametric model in which some parameters, such as those descriptive of the instrument response function (IRF), are wavelength-dependent, whereas others, such as the lifetime of a certain spectrally distinct component, underlay the data at all wavelengths. The presence of parameters that underlay the data at all wavelengths allows the application of global analysis techniques (*33*), which model wavelength-invariant parameters as a function of available data. The partitioned variable projection algorithm is well suited to the optimization of model parameters for global analysis models (*44*). The algorithm has the further advantage of estimating the standard error of parameter estimates, an advantage that is useful in model selection and validation. A compartmental model was used to describe the evolution of the spectrally distinct components in time. Global analysis was then applied to estimate the lifetime and relative concentration of each component at each wavelength in the data.

The femtosecond transient absorption data were first globally analyzed using a kinetic model consisting of sequentially interconverting evolution-associated difference spectra (EADS), i.e., $1 \rightarrow 2 \rightarrow 3 \rightarrow \ldots$, in which the arrows indicate successive monoexponential decays of increasing time constants, which can be regarded as the lifetime of each EADS. Such a sequential analysis quantifies the spectral evolution: from the sequential analysis the minimal number of lifetimes (and components) necessary to describe the data satisfactorily is determined. Using the sequential scheme with increasing lifetimes, these lifetimes and the EADS are estimated. The first EADS corresponds to the time zero difference spectrum. This procedure enables us to clearly estimate the time scales and visualize the evolution of the (excited and intermediate) states of the system.

To disentangle the contributions by the various molecular species in the spectral evolution, we performed a target analysis of time-resolved data. Target analysis involves the application of a compartmental model (i.e., a specific kinetic scheme) containing microscopic decay rates expressing intercompartmental transitions and may be used to test detailed hypotheses regarding the underlying kinetics. The spectrum associated with each component in a target analysis applied to difference absorption data is termed species-associated difference spectra (SADS). In contrast to the EADS, the SADS will represent the spectral signature of the pure molecular species and their kinetics after photon absorption. In this way, the reaction mechanism can be assessed in terms of discrete reaction intermediate states. Note that global and target analyses are complementary approaches and that their combination is well established (*33*).

RESULTS AND DISCUSSION

Absorption Spectra and Photocycle Time of Slr1694 Mutants. The UV−visible steady-state absorption spectra for dark and light states of the Slr1694 wild type (WT) and mutants are shown in Figure 2. The spectra of WT and W91F are practically identical, with absorption maxima at comparable amplitudes at 442 and 379 nm, assigned to the two lowest excited states S_1 and S_2 of FAD, respectively (Figure 2A). In addition, a vibronic shoulder at 465 nm is resolved. The Y8W mutant shows peaks at 372 and 439 nm with a shoulder at 461 nm and a different ratio between S_1 and S_2 bands. The absorption spectrum of the S28A mutant shows an overall red shift of the absorption with bands at 387 and 456 nm and a shoulder at 479 nm. Furthermore, the S_2 band is significantly higher than the S_1 band. YcgF from *E. coli*, also called Blrp, contains an alanine at position 28 in its WT form and is equivalent to the Slr1694 S28A mutant in this regard. YcgF shows a similar red-shifted steady-state absorption with S_2 and S_1 at 382 and 459 nm and a shoulder at 484 nm (*14*, *36*). The mutation may change the dipolar interaction between this polar residue and the isoalloxazine ring, resulting in a red shift of the UV−visible absorption. Alternatively, the FAD wave function may slightly extend over the serine in wild type, affecting the transition energy (*38*).

Upon blue light illumination, WT and the W91F and S28A mutants show a characteristic red shift of the absorption spectrum (Figure 2B). The Y8W mutant does not show any red-shifted absorption or other long-lived photoproduct. In W91F, the red-shifted spectrum thermally decays to the dark-adapted state in 223 s, which is about 50 times slower than in WT.

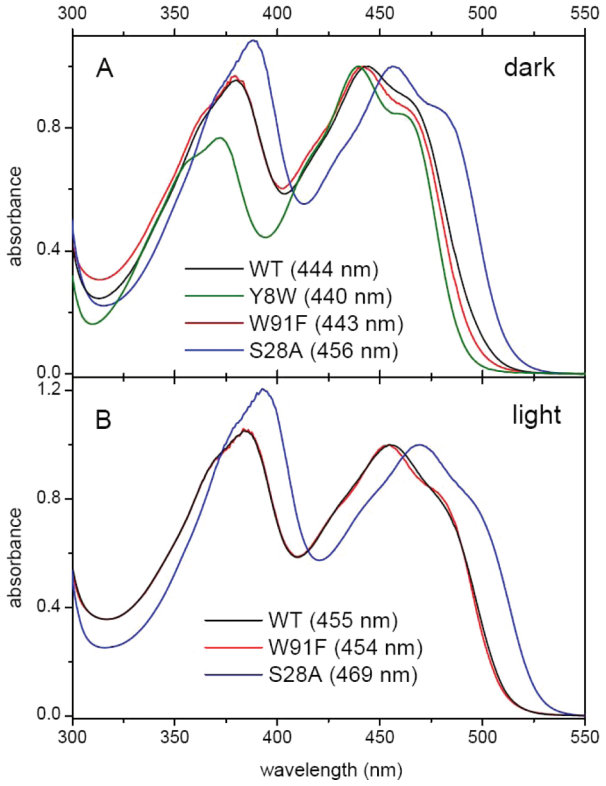

FIGURE 2: (A) Absorption spectra of Slr1694 wild type (black line) and W91F (red line), S28A (blue line), and Y8W mutants (olive line). (B) Absorption spectra of Slr1694 wild type (black line), W91F (red line), and S28A (blue line) in the signaling state. All spectra have been normalized to unity at the S_1 maximum.

This observation is quite remarkable given that in the AppA BLUF domain the corresponding mutation leads to acceleration of the photocycle (*37*). The S28A mutant has a dark recovery of 4 s, essentially the same as in WT.

Ultrafast Spectroscopy of Wild-Type Slr1694. Ultrafast transient absorption spectroscopy on wild-type Slr1694 was performed previously in our laboratory (*19*). The ultrafast experiments reported in this paper were performed on a different laser setup (see Materials and Methods). For reference and to check reproducibility, we performed experiments on WT Slr1694, presented in Figure SI1 (EADS) and Figure SI2 (kinetics) of the Supporting Information. The results were essentially identical to those we published before except that in the present experiments the amplitude of the EADS in the FAD ground state bleach region around 450 nm was about 30% larger, and that of the induced absorption near 690 nm was 10% larger. These differences probably arise from slightly different spectrospatial overlaps of pump and probe beams and therefore do not affect the interpretation of the spectra. The kinetics were virtually indistinguishable, indicating that the evolution in terms of molecular intermediates was identical between the two experiments.

Ultrafast Spectroscopy of the W91F Mutant. In the Slr1694 and AppA X-ray structures, the semiconserved residues W91 and W104 have been reported in two conformations, either close to the flavin ("W-in") or in a solvent-exposed position ("W-out") (*4*, *5*, *7*). In its "W-in" conformation, the indole ring of the tryptophan points toward the flavin at about 4 Å away in Slr1694 (Figure 1A)(*7*). In the AppA BLUF domain, the pyrrole nitrogen of W104 hydrogen bonds to FAD C4=O at a significantly closer distance of 3.3 Å (*4*).

Ultrafast transient absorption spectroscopy was applied to the W91F mutant of the Slr1694 BLUF domain from *Synechocystis* to study its reaction mechanism. The sample was excited at 400 nm, and the ensuing absorbance changes were monitored in a spectral window from 420 to 690 nm. The experimental results were globally analyzed in terms of a sequential kinetic scheme with monoexponentially decaying interconverting species. Figure 3A shows the result of the global analysis procedure in the form of evolution-associated difference spectra (EADS) for W91F in H_2O. Kinetic traces at selected wavelengths for W91F in H_2O and D_2O are shown in Figure SI3 of the Supporting Information. Five components were required to fit the data with lifetimes of 1.4 ps (2 ps in D_2O), 16 (16) ps, 90 (138) ps, 380 (590) ps, and nondecaying component. The first EADS (Figure 3A, black line) is formed within the instrument response function of ~120 fs and shows a ground state bleach near 450 nm, excited-state absorption around 520 nm, stimulated emission at 550 nm, and excited-state absorption at wavelengths longer than ~610 nm. It is associated with singlet excited flavin (FAD*). Similar spectral signatures for flavin in the lowest singlet excited state have been found for Slr1694 WT (*19*), Appa WT and mutants (*20*, *35*), flavin in solution (*45*), and FMN* in the LOV2 domain of phototropin (*46*). The first EADS evolves to the second EADS in 1.4 ps and involves minor spectral changes that include a loss of bleach near 470 nm and a slight blue shift of the stimulated emission band near 550 nm. This evolution can be assigned to a vibrational cooling process on the excited FAD chromophore in combination with excited-state decay (*19*, *35*, *47*).

The second EADS has a lifetime of 16 ps and evolves to the third EADS (blue line), which itself has a lifetime of 90 ps. The third EADS shows a decrease of ground state bleaching and stimulated emission, indicating decay of FAD*, and an increase of absorption near 600 nm. The latter indicates the presence of other molecular species that correspond to FAD radicals, as will be shown below. The fourth EADS (green line) rises in 90 ps and has a lifetime of 380 ps. It shows further decay of ground state bleach and stimulated emission features and a decay of the transient band at 600 nm. A prominent positive band has come up near 490 nm which is indicative of long-lived product ($BLUF_{RED}$, also referred to as Slr_{RED} in the specific case of Slr1694) formation (*19*). In the last, nondecaying EADS (magenta line), all signs of FAD* or FAD radical species have disappeared, and the difference spectrum corresponds to the red-shifted photoactivated state of BLUF domains, $BLUF_{RED}$, apart from a low-amplitude, broad absorption between 550 and 680 nm. The latter may correspond to a small fraction of FAD triplet states, as observed previously in the AppA BLUF domain (*20*, *35*). The overall spectral evolution of the W91F mutant in H_2O and D_2O is quite similar to that of wild-type Slr1694 (*19*, *21*).

Target Analysis of W91F: Assessment of the Reaction Dynamics. We have shown previously for WT Slr1694 that the EADS that follow from a sequential global analysis represent a mixture of molecular states (*19*, *22*). This was primarily related to the multiexponenential decay of FAD* observed in Slr1694. Such multiexponential excited-state decay was observed by means of time-resolved fluorescence spectroscopy, not only on Slr1694 (*22*) but also on the AppA BLUF domain (*20*, *35*, *37*, *48*), BlrB (*49*), and in TePixD (*24*). To extract the spectral signature of "pure" molecular species that underlie the molecular transformations, we applied a target analysis (*33*), using a kinetic scheme that took into account the multiphasic FAD* decay and two intermediates, Q_1 and Q_2, that are transiently populated and result in

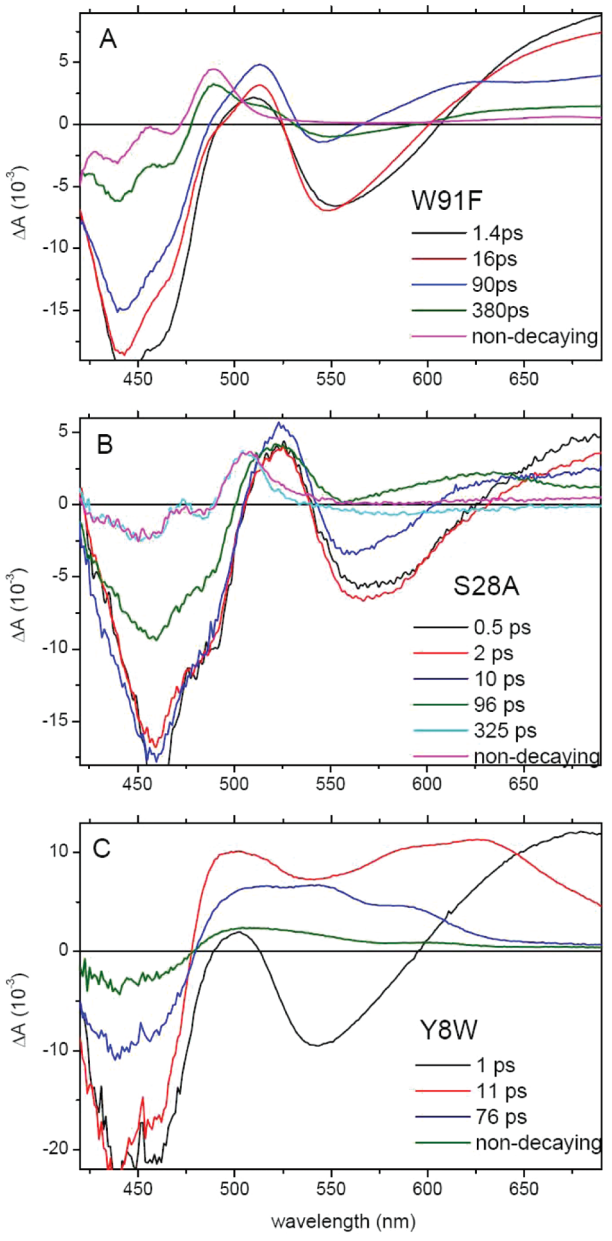

FIGURE 3: (A) Evolution-associated difference spectra (EADS) resulting from a global analysis on transient absorption experiments on the W91F mutant. (B) EADS of the S28A mutant. (C) EADS of the Y8W mutant. The excitation wavelength was 400 nm in all cases.

the long-lived red-shifted state $BLUF_{RED}$. We demonstrated that inclusion of two such intermediates between FAD* and $BLUF_{RED}$ was required for an adequate fit (*19*, *21*, *22*). Thus, the wild-type data were analyzed with a minimal model.

From the target analysis, species-associated difference spectra (SADS) were derived that corresponded to difference spectra of discrete reaction intermediates. Here, we have applied a similar procedure to the W91F mutant. The kinetic scheme is shown in Figure 4A and consists of eight compartments: four FAD* compartments that have an identical SADS, two intermediates, Q_1 and Q_2, a long-lived product $BLUF_{RED}$, and a FAD triplet state (FAD^T). This scheme is identical to that used for wild-type Slr1694 (*19*, *21*, *22*), except for the triplet compartment. Note that in a target analysis on the AppA BLUF domain such a triplet state was included (*20*, *35*). The transient absorption data of W91F in H_2O and D_2O were simultaneously analyzed with a common set of SADS, only allowing for small differences in the

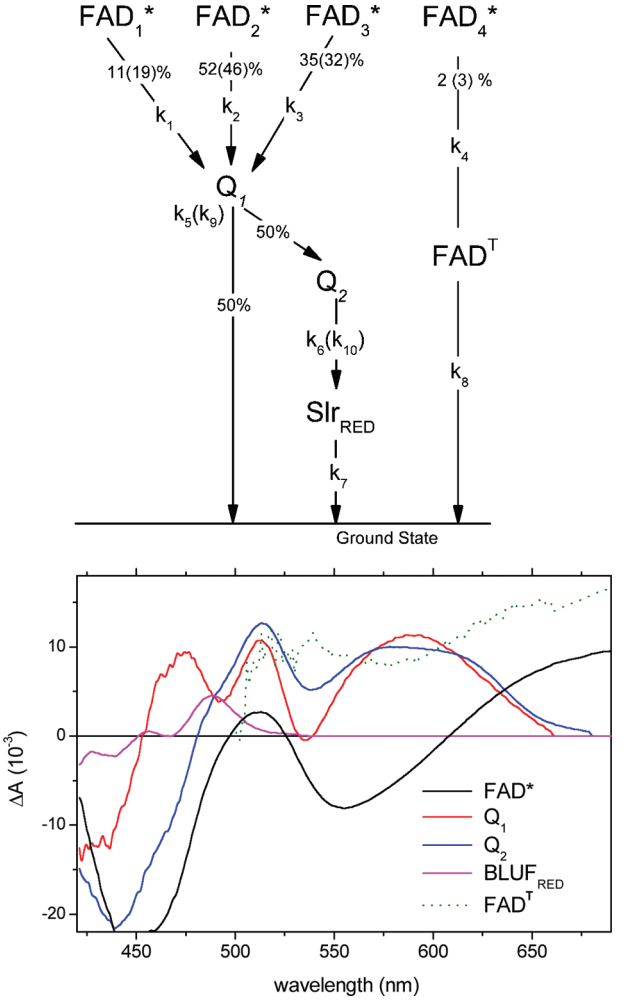

FIGURE 4: (A) Kinetic model applied in the target analysis for the W91F mutant. (B) Species-associated difference spectra (SADS) resulting from a target analysis.

FAD^*_{1-4} compartment fractions between H_2O and D_2O. The resulting SADS are shown in Figure 4B, whereas rate constants and fractions of FAD^*_{1-4} contributions are reported in Table 2. We note that the spectral constraints on the target analysis are in fact rather strict: two independent data sets (in H_2O and D_2O) are fitted to the same kinetic model that have essentially identical SADS, and only the rate constants that connect the compartments are allowed to vary freely. As compared to the sequential analysis, where there is total spectral and temporal freedom for the two data sets, this gives a significantly reduced free parameter space.

In Figure 4B, the black SADS is associated with FAD*. The target analysis indicates that the decay of FAD^*_{1-4} is highly multiexponential, with time constants of 2.3, 24, 250, and 3.3 ns. The time constants were set identical for W91F in H_2O and D_2O, which resulted in slightly different amplitudes for the four compartments (Table 2). The multiexponentiality most likely is caused by structural flexibility in the FAD binding pocket, particularly of the conserved electron donor Y8 (*13*, *26*). Such heterogeneity of the ground state was previously observed in wild-type Slr1694 (*19*, *22*), *Thermococcus elongatus* TePixD (*24*), and AppA and its mutants (*9*, *20*, *35*). The absence of an obvious H/D exchange effect on the decay of FAD^*_{1-4} indicates that FAD* is deactivated through electron transfer, as for wild-type Slr1694 (*19*, *21*, *22*).

Table 2: Rate Constant and Fractional Contributions Estimated for the W91F Mutant Using Target Analysis[a]

	FAD_1*	FAD_2*	FAD_3*	FAD_4*	Q_1	Q_2	Slr_{RED}	FAD^T
FAD_1*								
FAD_2*								
FAD_3*								
FAD_4*								
Q_1	k_1, 11(19)%	k_2, 52(46)%	k_3, 35(32)%		k_5 (k_9)			
Q_2					k_5 (k_9)			
Slr_{RED}						k_6 (k_{10})	k_7	
FAD^T				k_4, 2(3)%				k_8

$k_1 = 442 \times 10^{-3}$ ps^{-1}	$\tau_1 = (k_1)^{-1} = 2.26$ ps
$k_2 = 425 \times 10^{-4}$ ps^{-1}	$\tau_2 = (k_2)^{-1} = 23.5$ ps
$k_3 = 402 \times 10^{-5}$ ps^{-1}	$\tau_3 = (k_3)^{-1} = 250$ ps
$k_4 = 300 \times 10^{-6}$ ps^{-1}	$\tau_4 = (k_4)^{-1} = 3.3$ ns
$k_5 = 206 \times 10^{-3}$ ps^{-1}	${}^{H_2O}\tau_{Q_1} = (k_5)^{-1} = 4.8$ ps
$k_6 = 134 \times 10^{-4}$ ps^{-1}	${}^{D_2O}\tau_{Q_1} = (k_9)^{-1} = 11$ ps
$k_7 = 0.0$ ps^{-1}	${}^{H_2O}\tau_{Q_2} = (k_6)^{-1} = 75$ ps
$k_8 = 0.0$ ps^{-1}	${}^{D_2O}\tau_{Q_{2_1}} = (k_{10})^{-1} = 130$ ps
$k_9 = 934 \times 10^{-4}$ ps^{-1}	$\tau_{Slr_{RED}} = (k_7)^{-1} \rightarrow$ nd
$k_{10} = 786 \times 10^{-5}$ ps^{-1}	$\tau_{FAD^T} = (k_8)^{-1} \rightarrow$ nd

[a] Q_1 corresponds with $FAD^{\bullet-}-Y8^{\bullet+}$ and Q_2 with $FADH^{\bullet}-Y8^{\bullet}$. See text for details. nd: nondecaying.

FAD^*_{1-3} evolve to the first intermediate Q_1. The Q_1 SADS (red line) shows a positive band at 520 nm and a broad symmetric band near 590 nm. It resembles the absorption difference spectrum of the anionic flavin semiquinone ($FAD^{\bullet-}$) in a charge-transfer (CT) interaction, as previously observed in wild-type Slr1694 (*19*) and in certain flavoenzymes (*50*). As in the wild type, Q_1 is associated with a molecular species $FAD^{\bullet-} + Y8^{\bullet+}$ (*19*, *21*, *22*), Q_1 is short-lived, and its SADS is therefore hard to estimate. It decays in 5 ps (11 ps in D_2O), forming the second intermediate Q_2 at a yield of 50%. About half of the $FAD^{\bullet-} + Y8^{\bullet+}$ radical pairs decay to the ground state through charge recombination (*19*). The Q_2 SADS (blue line) has a broad absorption between 480 and 680 nm with maxima at 575 and 605 nm. This SADS is assigned to a neutral semiquinone flavin radical $FADH^{\bullet}$ (*19*, *51*) that is formed upon proton transfer from Y8 (*19*, *21*, *22*). Q_2 represents a neutral radical pair $FADH^{\bullet} + Y8^{\bullet}$. Radical pair recombination with ensuing decay of $FADH^{\bullet}$ occurs in 75 ps (130 ps in D_2O), forming the nondecaying $BLUF_{RED}$ species (magenta line), with its typical absorption peak at 489 nm, which is characteristic of the BLUF signaling state.

The decay of FAD* is highly multiexponential and distributed between a few picoseconds and ~250 ps in wild-type Slr1694 (*19*, *21*, *22*) and the W91F mutant, which is assigned to different conformational subpopulations of the tyrosine side chain having variations in the distance to FAD, with an ensuing distribution of electron transfer rates (*9*, *20*). According to the kinetic model of Figure 4 (upper) and that for wild-type Slr1694, a single proton transfer rate of about $(5\ ps)^{-1}$ governs protonation of $FAD^{\bullet-}$ to $FADH^{\bullet}$. This may seem difficult to understand because, given a flexible configuration in the FAD binding pocket, proton transfer is expected to exhibit a certain dispersion in rate constants as well, just as the Y8−FAD electron transfer process. Here, it should be realized that the $FAD^{\bullet-}$ anion is only short-lived, attains a low transient concentration, and is therefore difficult to detect. The extracted proton transfer time constant of $(5\ ps)^{-1}$ only follows from the FAD_1* and FAD_2* branches, where it results in a detectable transient FAD anion concentration. For the FAD_3* branch, proton transfer remains spectrally silent within the signal-to-noise ratio. However, the FAD_3* branch does contribute to $BLUF_{RED}$ formation, as becomes apparent as a slow phase of ~250 ps in the rise of the latter species. This process presumably proceeds through a $FADH^{\bullet}$ intermediate and hence involves proton transfer as indicated in the reaction model. However, we cannot exclude that, for this branch, proton transfer proceeds significantly slower than 5 ps.

As observed previously for wild-type Slr1694, a minor fraction of excited FAD (FAD^*_4) does not feed into the productive photocycle. The target analysis results in a lifetime of 3.3 ns for FAD^*_4. Given such a time scale, it is expected that a major part of this FAD* fraction undergoes intersystem crossing to the FAD triplet state (FAD^T, green SADS in Figure 4B (*46*)). Reliable spectral estimation of FAD^T is only possible in the part of the spectrum where its SADS is sensibly different from the other SADS. To estimate the FAD^T SADS, the ground state bleach part from 420 to 500 nm was set identical to that of the singlet excited state FAD* and a low weight was assigned to the FAD^T SADS between 420 and 500 nm assigned in the fitting procedure to avoid compensation effects with flavin ground state bleach present in the SADS of FAD^*_{1-4}, Q_1, Q_2, and Slr_{RED}. The resulting FAD^T SADS shows a broad, positive absorption from 500 to 690 nm, with a spectral shape that is similar to that observed in the AppA BLUF domain (*35*) and the LOV_1 and LOV_2 domains of phototropin (*46*, *52*, *53*).

No Evidence for Electron Transfer from Trp-91 in Slr1694. For the AppA BLUF domain, it was shown previously that the quantum yield of $BLUF_{RED}$ formation is ~40% higher in the W104F mutant (0.37) as compared to wild type (0.24) (*20*, *37*). This phenomenon was explained with a competition between a light-driven electron transfer from the conserved tryptophan (W104) to FAD and electron transfer from the conserved tyrosine, whereby the former represents a nonproductive deactivation channel (*20*, *37*). Upon removal of W104, this electron transfer pathway was eliminated, leading to a longer excited-state lifetime and increased $BLUF_{RED}$ quantum yield. To examine whether such phenomena occur in Slr1694 as well, Figure SI4 shows a comparison of the signal amplitudes of FAD* and $BLUF_{RED}$ for wild-type Slr1694 and the W91F mutant. The amplitudes of FAD* ground state bleach at early times at 450 nm

Table 3: Time Constants (in ps) from Target Analysis for Slr1694 Wild Type and W91F, Y8W, and S28A Mutants[a]

	WT	W91F	Y8W	S28A
^{hot}FAD*	nr	nr	nr	0.5
FAD_1*	6 (7)	2	1 (0.77)	5
FAD_2*	26 (28)	24	8	20
FAD_3*	92 (94)	250	nr	115
FAD_4*	335 (354)	3300	nr	nr
Q_1	6 (20)	5 (11)	10 (18)	37 (110)
Q_2	67 (160)	75 (130)	206 (332)	nr
Q_3	nr	nr	4300	nr
Slr_{RED}	6 s (20 s)	223 s	nph	5 s
FAD^T	nr	nd	nr	np

[a]Decay times of Slr_{RED} are indicated in seconds. nr, not relevant; nph, non-photocycling; nd, nondecaying.

and the $BLUF_{RED}$ induced absorption at 489 nm are similar for wild-type Slr1694 and the W91F mutant. This observation shows that the quantum yields for $BLUF_{RED}$ formation in wild type and W91F mutant are not significantly different in Slr1694 and amount to ca. 0.40 (*19*). Also, the FAD* lifetimes in wild type and W91F are quite similar, and the intermediates that lead to the red form, identified as Q_1 ($FAD^{\bullet-}-Y8^{\bullet+}$) and Q_2 ($FADH^{\bullet}-Y8^{\bullet}$), are formed and decay with essentially identical lifetimes compared to the WT (Table 3 and ref *19*).

The similarities in the photocycle and quantum yield for the signaling state formation demonstrate that W91 is not required for Slr1694 photoactivation nor does it provide a significant pathway for electron transfer to FAD that competes with productive electron transfer from Y8. This finding is consistent with our ultrafast IR results on Slr1694 (*22*) and a recent time-resolved fluorescence study on the Y8F mutant of *Thermosynechococcus* TePixD, which indicated no electron transfer from W91 to FAD up to a time scale of 100's of picoseconds (*24*).

For the AppA BLUF domain, the observation of electron transfer from W104 to FAD (*20*), along with tryptophan fluorescence (*25*) and NMR results (*9*), lended support to a "W-in" conformation of W104 in dark-state AppA. The absence of such a W91-FAD electron transfer process does, however, not necessarily imply that W91 assumes the "W-out" conformation in dark-state Slr1694. Inspection of the Slr1694 X-ray structure indicates that Trp91 in the "W-in" conformation is further away from FAD than in the AppA X-ray structure (*4*, *7*), which will result in a slower electron transfer rate in the former. Given that electron transfer from Tyr to FAD is much faster in Slr1694 than in AppA [~10 ps vs ~600 ps dominant conponents (*19*, *21*, *22*, *35*)], it is likely that electron transfer from Trp-91 cannot compete with electron transfer from Tyr-8 in Slr1694 and is therefore not observed. Thus, the issue whether W91 assumes a W-in or W-out conformation remains unsettled on the basis of the present results. We note that tryptophan fluorescence experiments on Slr1694 have indicated that W91 assumes a buried, "W-in" conformation in the dark (*7*).

The question arises as of why electron transfer from the conserved tyrosine to FAD is so much more efficient that that of the conserved tryptophan, in Slr1694 as well as the AppA BLUF domain, given that their distances to FAD are similar and Trp is often regarded as a better electron donor to flavin than Tyr. It is interesting in this regard to consider recent theoretical work by Stanley and co-workers in the context of photolyases and cryptochromes (*54*). Their time-dependent density functional theory calculations on flavin indicated that particular patches of the isoalloxazine ring, C6 and C7, that are in closest vicinity to the redox-active conserved tryptophan in photolyase, become electropositive upon light absorption. The authors proposed that this phenomenon constitutes an important physical−chemical determinant for catalytic light-driven electron transfer. Interestingly, in BLUF domains the conserved tyrosine is positioned close to the flavin xylene ring at about 4 Å, similar to the arrangement of tryptophan and FAD in photolyase. This observation supports the notion that efficient electron transfer from an aromatic side chain to flavin is promoted through positioning toward flavin C6 and C7 and provides a rationale for the more efficient electron transfer in BLUF domains from tyrosine to FAD as compared to tryptophan.

Ultrafast Spectroscopy of the S28A Mutant. From structural data on Slr1694 the semiconserved S28 is observed in two conformations of the side chain with one close to heterocyclic ring of the flavin chromophore, as shown in Figure 1D, and another coordinating the backbone (not shown). The near distances of the serine oxygen atom to the heteroatoms of the flavin range from 4.8 Å (C_2O) to 3.5 Å (N_5). The proximity of S28 to FAD suggests that S28 may act as a proton donor to FAD at some point in the photochemical reaction cycle.

Femtosecond transient absorption experiments were performed on the S28A mutant of the Slr1694 BLUF domain. The EADS that result from a sequential analysis of the time-resolved data are presented in Figure 3B, with kinetic traces at selected wavelengths for S28A in H_2O and D_2O shown in Figure SI5 of the Supporting Information. Six kinetic components were required to fit the data in H_2O (D_2O), with lifetimes of 0.5 ps, 2 (2.7) ps, 10 (16) ps, 96 (90) ps, and 325 (610) ps and a nondecaying component. A subpicosecond component could be resolved in this particular data set because of a cross-phase modulation artifact weaker than in the other mutants. However, due to the instability of the long-lived photoproduct of the S28A mutant, the overall S/N ratio of this particular data set is lower than those obtained on wild-type Slr1694 and other mutants. The 0.5 ps EADS (black line) represents a mixture of the initially excited S_2 and S_1 excited states of FAD (*35*). After internal conversion in 0.5 ps, the 2 ps EADS (red line) represents the lowest singlet excited state of FAD, denoted as FAD*. The third and fourth EADS with lifetimes of 10 ps (blue line) and 96 ps (green line) are a mixture of FAD* and flavin radical species absorbing in the central part of the spectrum at above 550 nm. The fifth, 325 ps EADS (cyan line) corresponds to mainly the long-lived $BLUF_{RED}$ photoproduct. The small-amplitude negative-going signal at ~580 nm is hardly resolved given the poor signal-to-noise ratio in this particular experiment. If significant at all, it may correspond to a small fraction of unbound FAD*. The sixth, nondecaying EADS (magenta line) represents the photoproduct $BLUF_{RED}$, which absorbs near 505 nm in this particular mutant. As for the W91F mutant, the overall spectral evolution of this mutant is similar to that of WT Slr1694 (*19*).

Target Analysis of S28A: Assessment of the Reaction Dynamics. For a more complete, quantitative understanding of the photochemistry of the S28A mutant, a target analysis has been applied to the time-resolved data. The kinetic scheme employed and the SADS resulting from the target analysis are displayed in Figure 5A. The kinetic scheme is similar to that of wild type and W91F, except that only one intermediate (Q_1) is used to connect FAD* to $BLUF_{RED}$. The lifetimes of each compartment are reported in Table 3; rate constants and

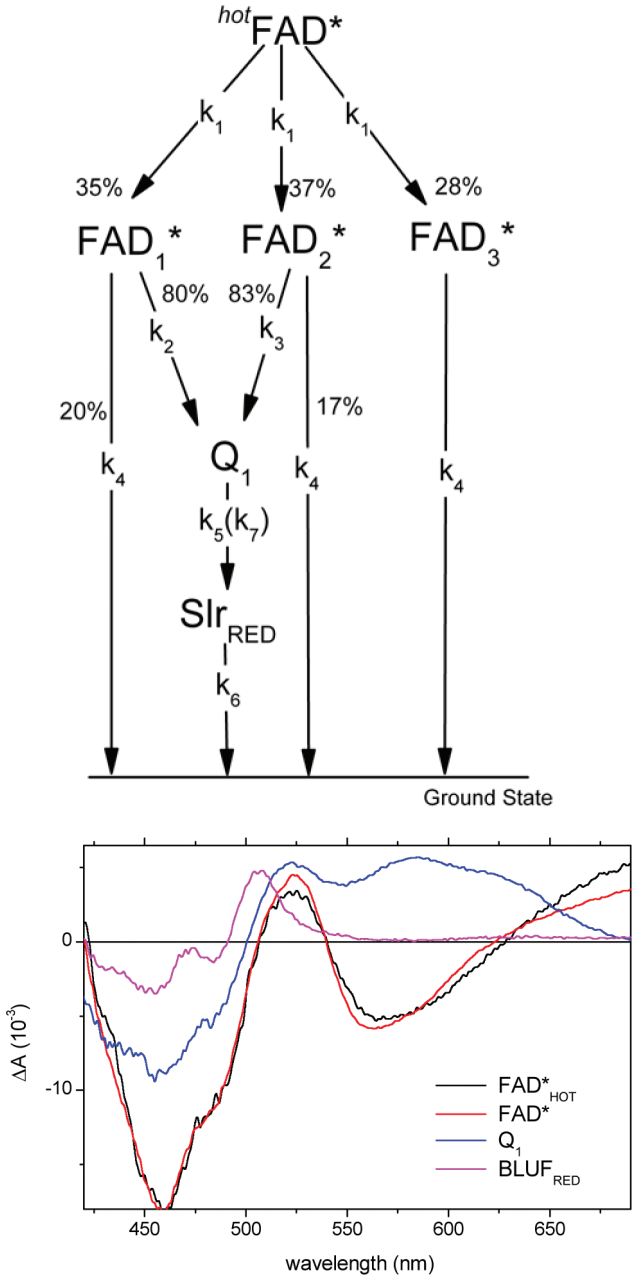

FIGURE 5: (A) Kinetic model applied in the target analysis for the S28A mutant. (B) Species-associated difference spectra (SADS) resulting from a target analysis.

fractional contributions are reported in Table 4. The FAD_{S1-S2} ($^{hot}FAD^*$, black line in Figure 5B) compartment decays on a subpicosecond time scale (0.5 ps) to populate FAD^*_{1-3}. These three singlet excited states of flavin have identical SADS (the red SADS, Figure 5B) but different decay times. $FAD^*_{1,2}$ relaxation occurs in 5 and 20 ps, mainly (~80%) through Q_1 and a minor fraction (~20%) directly to the ground state. FAD_3^* decays entirely to the ground state with a lifetime of 115 ps. The short FAD* lifetimes are similar to those of WT, as FAD^*_{1-2} decay in 5 and 20 ps and 6 and 26 ps in S28A and WT, respectively. The nonproductive component FAD_3^* has a lifetime of 115 ps in S28A, which is twice as short as in WT (335 ps; see comparison in Table 3). As for wild type and W91F, the decay of FAD^*_{1-3} does not show any effect of H/D exchange, indicating that FAD* is deactivated through electron transfer (*19*, *21*, *22*). Q_1 is populated from FAD^*_{1-2}. Its SADS (blue line) resembles the spectrum of the

Table 4: Rate Constant and Fractional Contributions Estimated for the S28A Mutant Using Target Analysis[a]

	$^{hot}FAD^*$	FAD_1^*	FAD_2^*	FAD_3^*	Q_1	Slr_{RED}
$^{hot}FAD^*$						
FAD_1^*	k_1, 35%	k_4, 20%				
FAD_2^*	k_1, 37%		k_4, 17%			
FAD_3^*	k_1, 28%			k_4		
Q_1		k_2, 80%	k_3, 83%			
Slr_{RED}					k_5 (k_7)	k_6

$k_1 = 217 \times 10^{-2}$ ps^{-1}	$\tau_{hot} = (k_1)^{-1} = 0.46$ ps
$k_2 = 216 \times 10^{-3}$ ps^{-1}	$\tau_1 = (k_2 + k_4)^{-1} = 4.5$ ps
$k_3 = 430 \times 10^{-4}$ ps^{-1}	$\tau_2 = (k_3 + k_4)^{-1} = 20$ ps
$k_4 = 870 \times 10^{-5}$ ps^{-1}	$\tau_3 = (k_4)^{-1} = 115$ ps
$k_5 = 268 \times 10^{-4}$ ps^{-1}	$^{H_2O}\tau_{Q_1} = (k_5)^{-1} = 37$ ps
$k_6 = 0.0$ ps^{-1}	$^{D_2O}\tau_{Q_1} = (k_7)^{-1} = 110$ ps
$k_7 = 907 \times 10^{-5}$ ps^{-1}	$\tau_{Slr_{RED}} = (k_6)^{-1} \rightarrow$ nd

[a] Q1 corresponds with $FADH^{\bullet}-Y8^{\bullet}$. See text for details. nd: nondecaying.

FAD neutral semiquinone ($FADH^{\bullet}$) that was previously identified in the wild-type Slr1694 (*19*) and the W91F mutant described above. $FADH^{\bullet}$ evolves to the $BLUF_{RED}$ compartment (magenta line) with a time constant of 37 ps in H_2O and 110 ps in D_2O.

In the target analysis of the WT and W91F mutant, two intermediates en route to the Slr_{RED} product were identified, $FAD^{\bullet-}$ and $FADH^{\bullet}$. For the S28A mutant, only one intermediate, $FADH^{\bullet}$, could be extracted from the time-resolved data. By its nature, the $FAD^{\bullet-}$ intermediate is short-lived (5−20 ps in WT and W91F in H_2O and D_2O, respectively) and difficult to detect. Given the relatively low signal-to-noise ratio in the S28A experiments, the $FAD^{\bullet-}$ intermediate may have escaped detection.

The S28A mutant shows a significant red shift in the UV−visible absorption spectrum, both in the dark and after illumination (Figure 2A,B). This may be due to disruption of a specific interaction (H-bond or dipolar interaction) between FAD and serine compared with the native S28 (*38*). Despite this obvious effect from the serine on the steady-state absorption properties, the photochemistry of the S28A mutant is very similar to that of wild type. Notably, however, the evolution from Q_1 to the Slr_{RED} product state is about two times faster in S28A as compared to WT and the W91F mutant (see Table 3). Like W91F, the S28A mutant does not exhibit a change of quantum yield of signaling state formation (Figure SI4, blue lines). In addition, the lifetime of the FAD singlet excited and the dark-state recovery of the red-shifted product state are not affected significantly (Table 3). We conclude that S28 is not required or significantly involved in the initial light-driven hydrogen bond switch reaction and does not, for instance, act as a proton donor to FAD after its initial reduction to $FAD^{\bullet-}$ by tyrosine. Possibly, S28 has a role in signal transmission to the molecular surface at a later stage of the photoreaction (*38*).

Ultrafast Spectroscopy of the Y8W Mutant. To investigate whether W can take up some of the roles of the conserved Y in BLUF domains, i.e., electron transfer and hydrogen bond switch capabilities, we constructed the Y8W mutant of Slr1694 and applied ultrafast spectroscopy. Since no crystal structure of the Y8W mutant is available, we introduced a tryptophan residue replacing Y8 by homology modeling (Figure 1C). The structural model of the Y8W mutant of Slr1694 was refined using the Swiss-Model homology-modeling server (*55*). As a template the PDB

file 2hfnA was used (*7*). The indole side chain is situated in the aromatic plane of the tyrosine residue, but the aromatic system is extended toward the xylene moiety of the isoalloxazine resulting in 0.5 Å shorter distance. However, if the phenolic oxygen atom of the tyrosine is considered, the distances for a dipolar or proton exchange interaction are still shorter in the wild-type protein. Especially the distance of the tyrosine phenolic oxygen to N5 is smaller than from the indole nitrogen. Note that W8 is unlikely to hydrogen bond with Q50, which makes it difficult to assess the conformation of the latter side chain.

The photochemistry of the Y8W mutant was investigated by femtosecond time-resolved absorption spectroscopy after 400 nm laser pulse excitation. The EADS resulting from global analysis are shown in Figure 3C. Kinetic traces at selected wavelengths for Y8W in H_2O and D_2O are shown in Figure SI6. Four components were required to adequately describe the time-resolved data, with lifetimes of 1 ps, 11 (18) ps, and 76 (100) ps in H_2O (D_2O) plus one nondecaying component. The black EADS in Figure 3C is similar to the initial EADS in wild type and the W91F and S28A mutants and is assigned to FAD*. This EADS decays in 1 ps to form the second EADS, which has a lifetime of 11 ps (red line). The second EADS shows a slightly reduced ground state bleach at 450 nm and a broad induced absorption at wavelengths longer than 475 nm, with a double-peak-like structure around 600 nm. In addition, a dip near 550 nm may be due to a remaining fraction of stimulated emission. We ascribe the second EADS to a mixture of a FAD radical and FAD* (see below). The second EADS spectrum evolves into the third EADS (blue line) in 11 ps (18 ps in D_2O). This EADS is characterized by a sharp drop in the FAD ground state bleach and induced absorption at longer wavelengths. With maxima at 550 and ~580 nm, the spectral shape of the induced absorption does not carry any spectral features associated with FAD* or the previous EADS. The third EADS evolves in 76 ps (100 ps in D_2O) into the long-lived EADS (green line) which does not decay on the time scale of our experiment. It is characterized by further reduction of the overall signal amplitude. It possesses an induced absorption near 520 nm that tails off to the red.

Target Analysis of Y8W: Identification of Three Different Radical Pairs. Upon replacement of Y8 with W, the long-lived signaling state is not formed, but photoinduced electron and proton transfer to FAD still occurs. To better understand the photochemical events in the Y8W mutant, the time-resolved data were subjected to a target analysis using the kinetic scheme displayed in Figure 6A. The scheme was chosen because it employs the minimum number of compartments (five), allows a physically reasonable interpretation, and provides a low root-mean-square error. Furthermore, with this model, the kinetic isotope effects on the rate constants are consistent with the physical−chemical nature of the FAD molecular species that correspond with the various SADS (*vide infra*). We note that the model is not uniquely suited to describe the data; however, we did not find an equally simple or simpler model that results in reasonable SADS. Hence, the parsimony principle dictates the choice of model presented in Figure 6A.

In the analysis, we identified four different molecular species, $FAD^*_{1,2}$, Q_1, Q_2, and Q_3. Note that because the Y8W photochemistry is so much different from that of wild type, Q_1 and Q_2 do not necessarily bear a direct relationship to Q_1 and Q_2 identified in wild-type Slr1694 BLUF (*19*, *21*, *22*). The SADS that result from the target analysis are reported in Figure 6B.

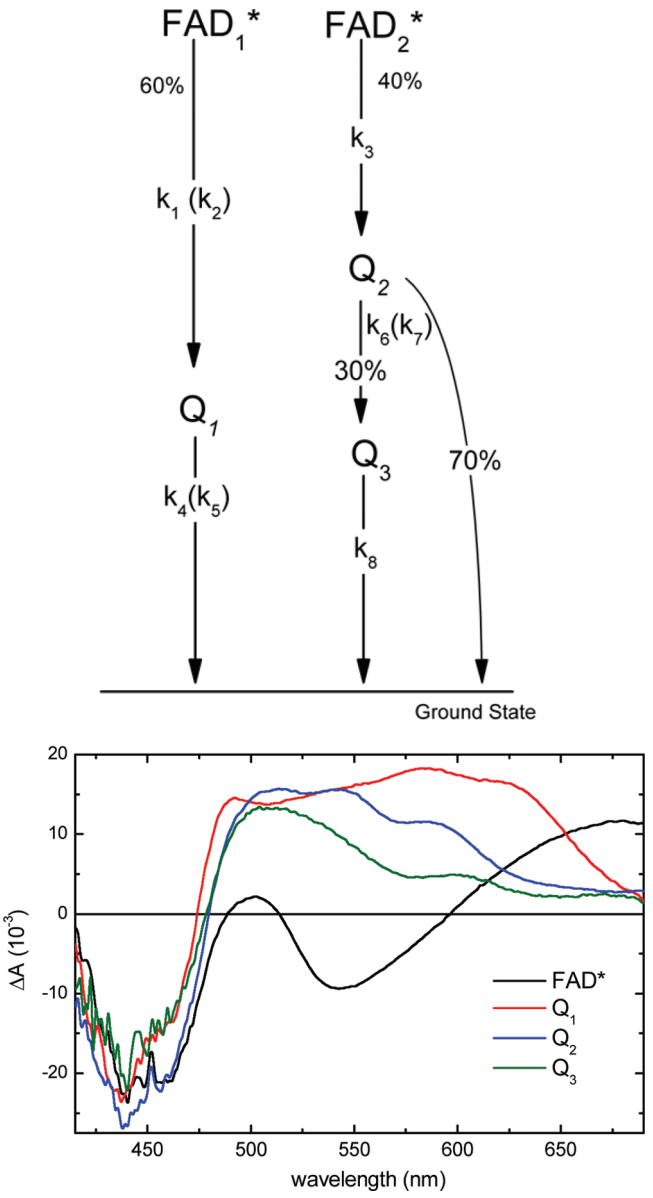

FIGURE 6: (A) Kinetic model applied in the target analysis for the Y8W Slr1694 mutant. (B) Species-associated difference spectra (SADS) resulting from a target analysis.

The $FAD^*_{1,2}$ SADS (black line) is essentially identical to those resolved for the W91F and S28A mutants (Figure 4B and Figure 5B, respectively). FAD^*_1 evolves to Q_1 (red SADS) in about 1 ps. Q_1 is characterized by a broad positive absorption spanning from 475 to 685 nm with peaks at 480, 585, and 625 nm. It resembles the absorption of a neutral semiquinone flavin radical, $FADH^\bullet$, that is red shifted in comparison to $FADH^\bullet$ in WT Slr1694. Q_1 recombines to the ground state showing a significant H/D exchange effect (10 and 18 ps in H_2O and D_2O, respectively). The latter observation indicates that radical pair recombination, probably involving hydrogen back-shuttling from FAD to the electron/proton donor, occurs.

Interestingly, the decay of FAD^*_1 is slightly faster in D_2O (0.77 ps) as compared to H_2O (1.1 ps), which implies that FAD^*_1 decay is subject to an inverted kinetic isotope effect (KIE). This phenomenon can be observed in the kinetics (Figure SI7, Supporting Information), where the decay of stimulated emission (545 nm) and the rise of the radical intermediate (605 nm) are slightly faster in the Y8W mutant in D_2O as compared to

H_2O. A KIE is unexpected on the FAD* lifetime because in BLUF domains electron transfer usually is considered to constitute the primary photochemical reaction (*19*, *20*, *22*, *23*, *48*). In addition, if proton or hydrogen transfer underlies FAD^*_1 in Figure 6A deactivation, one would under most circumstances expect a slowdown of the reaction upon H/D exchange, not a speeding up. Inverted KIE's have been reported in the literature (*56*, *57*). If in Y8W the decay of FAD^*_1 indeed corresponds to electron transfer, its fast rate of $\sim(1\text{ ps})^{-1}$ could be mediated by specific collective nuclear motions, as for instance shown for the photosynthetic reaction center (*58*, *59*). A downshift of such nuclear motions upon H/D exchange may result in an increased coupling with the charge separated state, effectively speeding up the electron transfer rate. The inverted KIE phenomenon in the Y8W mutant requires additional investigation and will not be further discussed here.

FAD^*_2, which represents 40% of the excited-state decay, evolves via rate constant k_3 $(8\text{ ps})^{-1}$ to form Q_2 (blue SADS). A 30% fraction of Q_2 decays with a rate constant k_6 (k_7 in D_2O) to form Q_3 (green SADS), whereas 70% recombines to the ground state (Table 3, kinetic scheme in Figure 6A, and Table 5). The Q_2 SADS shows a ground state bleach around 450 nm and a positive absorption for wavelengths longer than 480 nm, with three peaks at 510, 547, and 585 nm. As for Q_1, the ground state bleach indicates that Q_2 is associated with a flavin species. The absorption maxima at 547 and 585 nm resemble the $FADH^\bullet$ spectrum identified in wild-type Slr1694 (*19*). The observation of an absorption at 500 nm that is equally high or higher than the maximum at 547 and 585 nm indicates that other molecular species may be involved in this SADS. The absorption near 500 nm probably corresponds to a neutral tryptophanyl radical $W^\bullet$ (*60*), so that Q_2 corresponds to $FADH^\bullet-W^\bullet$.

The Q_3 SADS (green line) features the flavin ground state bleach near 450 nm and an induced absorption above 480 nm. It is formed from Q_2 with a yield of 30% and recombines to the ground state in 4.3 ns. The Q_3 species is spectroscopically very similar to a species called "R" in the AppA Y21I mutant (*20*). The latter species was tentatively assigned to a $FAD^{\bullet-}$ radical, possibly in combination with a $W^\bullet$ tryptophanyl neutral radical ($FAD^{\bullet-}-W^\bullet$) which both absorb around 520 nm (*50*, *60*). Alternatively, the low absorption near 600 nm may be due to a $W^{\bullet+}$ radical cation (*60*), consistent with a $FAD^{\bullet-}-W^{\bullet+}$ radical pair.

Electron Transfer Pathways in the Y8W Mutant. In contrast to other BLUF domains, the different FAD* decay phases of the Y8W mutant feed into distinct reaction pathways, leading to different transient intermediates. In Y8W, two separate deactivation pathways for the excited flavin are observed. The FAD^*_1 deactivation pathway is fast ($\sim$ 1 ps) and involves $\sim$60% of the initially excited flavin population, which results in transient $FADH^\bullet$ neutral radical formation. The second deactivation pathway for the photoexcited flavin FAD^*_2 is slower and involves the remaining $\sim$40%. FAD^*_2 evolves to neutral flavin semiquinone Q_2 ($FADH^\bullet$) in 8 ps, which, in turn, evolves in an anionic semiquinone Q_3 ($FAD^{\bullet-}$) in 206 ps (332 ps in D_2O; see Table 1 and Table 5). Notably, Q_1 and Q_2 both correspond to $FADH^\bullet$, but the former is 40 nm red shifted with respect to the latter, which indicates different interactions with the protein matrix, possibly via alternative hydrogen bond patterns.

The question arises whether Y8 or W91 acts as a redox partners to FAD in the Y8W photochemistry. In wild-type Slr1694, W91 does not participate or hardly participates in electron transfer to FAD (see the comparison between wild type and W91F above). In addition, in the Y8F mutant of the essentially identical *Thermosynechococcus* TePixD BLUF domain, no electron transfer from W91 to FAD was found to occur (*24*). Thus, most likely only W8 acts as electron and proton donor to FAD in the Y8W mutant in the FAD1* and FAD2* branches. Therefore, Q_1 most likely corresponds to $FADH^\bullet-W8^\bullet$, Q_2 corresponds to $FADH^\bullet-W8^\bullet$, and Q_3 corresponds either to $FAD^{\bullet-}-W8^\bullet$ or to $FAD^{\bullet-}-W8^{\bullet+}$. It should be noted, however, that the FAD_2* electron/proton transfer pathway is spectrally and temporally remarkably similar to that observed in the Y21I mutant of AppA (the "Q" and "R" intermediates in ref *20*), where W104 acted as the sole electron donor. Thus, W91 cannot entirely be excluded as a FAD redox partner in this deactivation branch.

Table 5: Rate Constant and Fractional Contributions Estimated for the Y8W Mutant Using Target Analysis[a]

	FAD_1*	FAD_2*	Q_1	Q_2	Q_3
FAD_1*					
FAD_2*					
Q_1	k_1 (k_2), 60%		k_4 (k_5)		
Q_2		k_3, 40%		k_6 (k_7), 70%	
Q_3				k_6 (k_7), 30%	k_8

$k_1 = 885 \times 10^{-3}\text{ ps}^{-1}$	$\tau_1 = (k_1)^{-1} = 1.1$ ps
$k_2 = 1298 \times 10^{-3}\text{ ps}^{-1}$	$\tau_2 = (k_2)^{-1} = 0.77$ ps
$k_3 = 1241 \times 10^{-4}\text{ ps}^{-1}$	$\tau_3 = (k_3)^{-1} = 8.0$ ps
$k_4 = 1035 \times 10^{-4}\text{ ps}^{-1}$	${}^{H_2O}\tau_{Q_1} = (k_4)^{-1} = 9.7$ ps
$k_5 = 565 \times 10^{-4}\text{ ps}^{-1}$	${}^{D_2O}\tau_{Q_1} = (k_5)^{-1} = 17.7$ ps
$k_6 = 485 \times 10^{-5}\text{ ps}^{-1}$	${}^{H_2O}\tau_{Q_2} = (k_6)^{-1} = 206$ ps
$k_7 = 301 \times 10^{-5}\text{ ps}^{-1}$	${}^{D_2O}\tau_{Q_2} = (k_7)^{-1} = 332$ ps
$k_8 = 2315 \times 10^{-7}\text{ ps}^{-1}$	$\tau_{Q_3} = (k_8)^{-1} = 4.3$ ns

[a] Q_1 corresponds with $FADH^\bullet-W8^\bullet$, Q2 with $FADH^\bullet-W8^\bullet$, and Q3 with $FAD^{\bullet-}-W8\bullet$ or $FAD^{\bullet-}-W8^{\bullet+}$. See text for details.

CONCLUSIONS

We have utilized ultrafast spectroscopy to characterize the photochemistry of Slr1694 mutants in which the putative electron and proton donors S28, W91, and Y8 have been removed and replaced by side chains with altered reactivity. The key residue for primary electron transfer, Y8, was substituted by tryptophan to verify if this side chain can transfer electrons and protons to FAD and possibly stabilize reaction intermediates for further studies. The conformational heterogeneity in the Y8W mutant results in two distinct deactivation pathways for the excited flavin. These pathways, characterized by different dynamics, are interpreted as distinct protein populations with two different, nearly isoenergetic conformations of the introduced tryptophan. The introduced W is likely to act as electron and proton donor to FAD to result in a short-lived radical pair that recombines on the picosecond to (sub)nanosecond time scale. The introduced W lacks the ability to stabilize the BLUF signaling state or any long-lived chemical species.

Removal of the hydroxyl group of the semiconserved side chain S28 resulted in photoactivation dynamics that revealed only one reaction intermediate, assigned to a FAD neutral semiquinone. Because the decay of the excited flavin is not sensitive to H/D exchange, electron transfer from Y8 to FAD is considered to be the rate-limiting event as in wild-type Slr1694. The quantum yield of signaling state formation and dark state

recovery remains comparable with that found for the wild type. Overall, our findings indicate that S28 does not play a vital role for the photoactivation of the Slr1694 protein at an early stage. The BLUF domain of YcgF from *E. coli* does not contain serine a this position and is strikingly similar to the S28A mutant with respect to its red-shifted absorption of both the dark and signaling state (*14*, *36*).

The transient absorption measurement on the W91F mutant finally showed that in Slr1694 W91 hardly participates in the photoactivation process, since photochemistry and quantum yield of the signaling state remain unchanged by this mutation. Besides, a longer living flavin excited state results in a formation of a small amount of flavin triplet. The dark recovery time is significantly increased. The results from ultrafast studies on mutated BLUF domains enabled us to rule out a general role in the initial photochemistry of two semiconserved amino acids, S28 and W91, for other so far investigated related BLUF proteins.

SUPPORTING INFORMATION AVAILABLE

EADS of a global analysis on transient absorption data of wild-type Slr1694 on two different transient absorption spectroscopy setups; kinetic traces at selected wavelengths of the W91F, S28A, and Y8F mutants in H_2O and D_2O; estimation of the quantum yield of $BLUF_{RED}$ formation in the W91F and S28A mutants. This material is available free of charge via the Internet at http://pubs.acs.org.

REFERENCES

1. Gomelsky, M., and Klug, G. (2002) BLUF: a novel FAD-binding domain involved in sensory transduction in microorganisms. *Trends Biochem. Sci. 27*, 497–500.
2. Iseki, M., Matsunaga, S., Murakami, A., Ohno, K., Shiga, K., Yoshida, K., Sugai, M., Takahashi, T., Hori, T., and Watanabe, M. (2002) A blue-light-activated adenylyl cyclase mediates photoavoidance in *Euglena gracilis*. *Nature 415*, 1047–1051.
3. Masuda, S., and Bauer, C. E. (2002) AppA is a blue light photoreceptor that antirepresses photosynthesis gene expression in *Rhodobacter sphaeroides*. *Cell 110*, 613–623.
4. Anderson, S., Dragnea, V., Masuda, S., Ybe, J., Moffat, K., and E. Bauer, C. (2005) Structure of a novel photoreceptor, the BLUF domain of AppA from *Rhodobacter sphaeroides*. *Biochemistry 44*, 7998–8005.
5. Jung, A., Domratcheva, T., Tarutina, M., Wu, Q., Ko, W. H., Shoeman, R. L., Gomelsky, M., Gardner, K. H., and Schlichting, I. (2005) Structure of a bacterial BLUF photoreceptor: insights into blue light-mediated signal transduction. *Proc. Natl. Acad. Sci. U.S.A. 102*, 12350–12355.
6. Jung, A., Reinstein, J., Domratcheva, T., Shoeman, R. L., and Schlichting, I. (2006) Crystal structures of the AppA BLUF domain photoreceptor provide insights into blue light-mediated signal transduction. *J. Mol. Biol. 362*, 717–732.
7. Yuan, H., Anderson, S., Masuda, S., Dragnea, V., Moffat, K., and Bauer, C. E. (2006) Crystal structures of the *Synechocystis* photoreceptor Slr1694 reveal distinct structural states related to signaling. *Biochemistry 45*, 12687–12694.
8. Kita, A., Okajima, K., Morimoto, Y., Ikeuchi, M., and Miki, K. (2005) Structure of a cyanobacterial BLUF protein, Tll0078, containing a novel FAD-binding blue light sensor domain. *J. Mol. Biol. 349*, 1–9.
9. Grinstead, J. S., Hsu, S. T. D., Laan, W., Bonvin, A. M. J. J., Hellingwerf, K. J., Boelens, R., and Kaptein, R. (2006) The solution structure of the AppA BLUF domain: insight into the mechanism of light-induced signaling. *ChemBioChem 7*, 187–193.
10. Wu, Q., Ko, W. H., and Gardner, K. H. (2008) Structural requirements for key residues and auxiliary portions of a BLUF domain. *Biochemistry 47*, 10271–10280.
11. Wu, Q., and Gardner, K. H. (2009) Structure and insight into blue light-induced changes in the BlrP1 BLUF domain. *Biochemistry 48*, 2620–2629.
12. Barends, T. R. M., Hartmann, E., Griese, J. J., Beitlich, T., Kirienko, N. V., Ryjenkov, D. A., Reinstein, J., Shoeman, R. L., Gomelsky, M., and Schlichting, I. (2009) Structure and mechanism of a bacterial light-regulated cyclic nucleotide phosphodiesterase. *Nature 459*, 1015–U150.
13. Grinstead, J. S., Avila-Perez, M., Hellingwerf, K. J., Boelens, R., and Kaptein, R. (2006) Light-induced flipping of a conserved glutamine sidechain and its orientation in the AppA BLUF domain. *J. Am. Chem. Soc. 128*, 15066–15067.
14. Hasegawa, K., Masuda, S., and Ono, T. A. (2006) Light induced structural changes of a full-length protein and its BLUF domain in YcgF(Blrp), a blue-light sensing protein that uses FAD (BLUF). *Biochemistry 45*, 3785–3793.
15. Masuda, S., Hasegawa, K., Ishii, A., and Ono, T. A. (2004) Light-induced structural changes in a putative blue-light receptor with a novel FAD binding fold sensor of blue-light using FAD (BLUF); Slr1694 of *Synechocystis* sp. PCC6803. *Biochemistry 43*, 5304–5313.
16. Takahashi, R., Okajima, K., Suzuki, H., Nakamura, H., Ikeuchi, M., and Noguchi, T. (2007) FTIR study on the hydrogen bond structure of a key tyrosine residue in the flavin-binding blue light sensor TePixD from *Thermosynechococcus elongatus*. *Biochemistry 46*, 6459–6467.
17. Unno, M., Masuda, S., Ono, T. A., and Yamauchi, S. (2006) Orientation of a key glutamine residue in the BLUF domain from AppA revealed by mutagenesis, spectroscopy, and quantum chemical calculations. *J. Am. Chem. Soc. 128*, 5638–5639.
18. Unno, M., Sano, R., Masuda, S., Ono, T. A., and Yamauchi, S. (2005) Light-induced structural changes in the active site of the BLUF domain in AppA by Raman spectroscopy. *J. Phys. Chem. B 109*, 12620–12626.
19. Gauden, M., van Stokkum, I. H. M., Key, J. M., Lührs, D. C., van Grondelle, R., Hegemann, P., and Kennis, J. T. M. (2006) Hydrogen-bond switching through a radical pair mechanism in a flavin-binding photoreceptor. *Proc. Natl. Acad. Sci. U.S.A. 103*, 10895–10900.
20. Gauden, M., Grinstead, J. S., Laan, W., van Stokkum, I. H. M., Avila-Perez, M., Toh, K. C., Boelens, R., Kaptein, R., van Grondelle, R., Hellingwerf, K. J., and Kennis, J. T. M. (2007) On the role of aromatic side chains in the photoactivation of BLUF domains. *Biochemistry 46*, 7405–7415.
21. Kennis, J. T. M., and Groot, M. L. (2007) Ultrafast spectroscopy of biological photoreceptors. *Curr. Opin. Struct. Biol. 17*, 623–630.
22. Bonetti, C., Mathes, T., van Stokkum, I. H. M., Mullen, K. M., Groot, M. L., van Grondelle, R., Hegemann, P., and Kennis, J. T. M. (2008) Hydrogen bond switching among flavin and amino acid side chains in the BLUF photoreceptor observed by ultrafast infrared spectroscopy. *Biophys. J. 95*, 4790–4802.
23. Dragnea, V., Waegele, M., Balascuta, S., Bauer, C. E., and Dragnea, B. (2005) Time-resolved spectroscopic studies of the AppA blue-light receptor BLUF domain from *Rhodobacter sphaeroides*. *Biochemistry 44*, 15978–15985.
24. Shibata, Y., Murai, Y., Satoh, Y., Fukushima, Y., Okajima, K., Ikeuchi, M., and Itoh, S. (2009) Acceleration of electron-transfer-induced fluorescence quenching upon conversion to the signaling state in the blue-light receptor, TePixD, from *Thermosynechococcus elongatus*. *J. Phys. Chem. B 113*, 8192–8198.
25. Toh, K. C., van Stokkum, I. H. M., Hendriks, J., Alexandre, M. T. A., Arents, J. C., Perez, M. A., van Grondelle, R., Hellingwerf, K. J., and Kennis, J. T. M. (2008) On the signaling mechanism and the absence of photoreversibility in the AppA BLUF domain. *Biophys. J. 95*, 312–321.
26. Sadeghian, K., Bocola, M., and Schutz, M. (2008) A conclusive mechanism of the photoinduced reaction cascade in blue light using flavin photoreceptors. *J. Am. Chem. Soc. 130*, 12501–12513.
27. Domratcheva, T., Grigorenko, B. L., Schlichting, I., and Nemukhin, A. V. (2008) Molecular models predict light-induced glutamine tautomerization in BLUF photoreceptors. *Biophys. J. 94*, 3872–3879.
28. Obanayama, K., Kobayashi, H., Fukushima, K., and Sakurai, M. (2008) Structures of the chromophore binding sites in BLUF domains as studied by molecular dynamics and quantum chemical calculations. *Photochem. Photobiol. 84*, 1003–1010.
29. Ishikita, H. (2008) Light-induced hydrogen bonding pattern and driving force of electron transfer in AppA BLUF domain photoreceptor. *J. Biol. Chem. 283*, 30618–30623.
30. Masuda, S., Hasegawa, K., and Ono, T. A. (2005) Tryptophan at position 104 is involved in transforming light signal into changes of beta-sheet structure for the signaling state in the BLUF domain of AppA. *Plant Cell Physiol. 46*, 1894–1901.
31. Masuda, S., Hasegawa, K., Ohta, H., and Ono, T. A. (2008) Crucial role in light signal transduction for the conserved Met93 of the BLUF protein PixD/Slr1694. *Plant Cell Physiol. 49*, 1600–1606.

32. Yuan, H., and Bauer, C. E. (2008) PixE promotes dark oligomerization of the BLUF photoreceptor PixD. *Proc. Natl. Acad. Sci. U.S.A. 105*, 11715–11719.
33. van Stokkum, I. H. M., Larsen, D. S., and van Grondelle, R. (2004) Global and target analysis of time-resolved spectra. *Biochim. Biophys. Acta 1657*, 82–104.
34. Okajima, K., Yoshihara, S., Fukushima, Y., Geng, X. X., Katayama, M., Higashi, S., Watanabe, M., Sato, S., Tabata, S., Shibata, Y., Itoh, S., and Ikeuchi, M. (2005) Biochemical and functional characterization of BLUF-type flavin-binding proteins of two species of cyanobacteria. *J. Biochem. 137*, 741–750.
35. Gauden, M., Yeremenko, S., Laan, W., van Stokkum, I. H. M., Ihalainen, J. A., van Grondelle, R., Hellingwerf, K. J., and Kennis, J. T. M. (2005) Photocycle of the flavin-binding photoreceptor AppA, a bacterial transcriptional antirepressor of photosynthesis genes. *Biochemistry 44*, 3653–3662.
36. Rajagopal, S., Key, J. M., Purcell, E. B., Boerema, D. J., and Moffat, K. (2004) Purification and initial characterization of a putative blue light-regulated phosphodiesterase from *Escherichia coli*. *Photochem. Photobiol. 80*, 542–547.
37. Laan, W., Gauden, M., Yeremenko, S., van Grondelle, R., Kennis, J. T. M., and Hellingwerf, K. J. (2006) On the mechanism of activation of the BLUF domain of AppA. *Biochemistry 45*, 51–60.
38. Gotze, J., and Saalfrank, P. (2009) Serine in BLUF domains displays spectral importance in computational models. *J. Photochem. Photobiol., B 94*, 87–95.
39. Okajima, K., Fukushima, Y., Suzuki, H., Kita, A., Ochiai, Y., Katayama, M., Shibata, Y., Miki, K., Noguchi, T., Itoh, S., and Ikeuchi, M. (2006) Fate determination of the flavin photoreceptions in the cyanobacterial blue light receptor TePixD (T110078). *J. Mol. Biol. 363*, 10–18.
40. Kraft, B. J., Masuda, S., Kikuchi, J., Dragnea, V., Tollin, G., Zaleski, J. M., and Bauer, C. E. (2003) Spectroscopic and mutational analysis of the blue-light photoreceptor AppA: a novel photocycle involving flavin stacking with an aromatic amino acid. *Biochemistry 42*, 6726–6734.
41. Laan, W., van der Horst, M. A., van Stokkum, I. H., and Hellingwerf, K. J. (2003) Initial characterization of the primary photochemistry of AppA, a blue-light-using flavin adenine dinucleotide-domain containing transcriptional antirepressor protein from *Rhodobacter sphaeroides*: a key role for reversible intramolecular proton transfer from the flavin adenine dinucleotide chromophore to a conserved tyrosine? *Photochem. Photobiol. 78*, 290–297.
42. Zirak, P., Penzkofer, A., Lehmpfuhl, C., Mathes, T., and Hegemann, P. (2007) Absorption and emission spectroscopic characterization of blue-light receptor Slr1694 from *Synechocystis* sp. PCC6803. *J. Photochem. Photobiol., B 86*, 22–34.
43. Berera, R., van Grondelle, R., and Kennis, J. T. M. (2009) Ultrafast transient absorption spectroscopy: principles and application to photosynthetic systems. *Photosynth. Res. 101*, 105–118.
44. Mullen, K. M., and van Stokkum, I. H. M. (2007) TIMP: an R package for modeling multi-way spectroscopic measurements. *J. Stat. Software 18*.
45. Stanley, R. J. (2001) Advances in flavin and flavoprotein optical spectroscopy. *Antioxid. Redox Signaling 3*, 847–866.
46. Kennis, J. T. M., Crosson, S., Gauden, M., van Stokkum, I. H. M., Moffat, K., and van Grondelle, R. (2003) Primary reactions of the LOV2 domain of phototropin, a plant blue-light photoreceptor. *Biochemistry 42*, 3385–3392.
47. Wolf, M. M. N., Schumann, C., Gross, R., Domratcheva, T., and Diller, R. (2008) Ultrafast infrared spectroscopy of riboflavin: dynamics, electronic structure, and vibrational mode analysis. *J. Phys. Chem. B 112*, 13424–13432.
48. Zirak, P., Penzkofer, A., Schiereis, T., Hegemann, P., Jung, A., and Schlichting, I. (2005) Absorption and fluorescence spectroscopic characterization of BLUF domain of AppA from *Rhodobacter sphaeroides*. *Chem. Phys. 315*, 142–154.
49. Zirak, P., Penzkofer, A., Schiereis, T., Hegemann, P., Jung, A., and Schlichting, I. (2006) Photodynamics of the small BLUF protein BlrB from *Rhodobacter sphaeroides*. *J. Photochem. Photobiol., B 83*, 180–194.
50. Miura, R. (2001) Versatility and specificity in flavoenzymes: control mechanisms of flavin reactivity. *Chem. Rec. 1*, 183–194.
51. Müller, F., Brüstlein, M., Hemmerich, P., Massey, V., and Walker, W. H. (1972) Light-absorption studies on neutral flavin radicals. *Eur. J. Biochem. 25*, 573–580.
52. Kottke, T., Heberle, J., Hehn, D., Dick, B., and Hegemann, P. (2003) Phot-LOV1: Photocycle of a blue-light receptor domain from the green alga *Chlamydomonas reinhardtii*. *Biophys. J. 84*, 1192–1201.
53. Swartz, T. E., Corchnoy, S. B., Christie, J. M., Lewis, J. W., Szundi, I., Briggs, W. R., and Bogomolni, R. A. (2001) The photocycle of a flavin-binding domain of the blue light photoreceptor phototropin. *J. Biol. Chem. 276*, 36493–36500.
54. Kodali, G., Siddiqui, S. U., and Stanley, R. J. (2009) Charge redistribution in oxidized and semiquinone *E. coli* DNA photolyase upon photoexcitation: stark spectroscopy reveals a rationale for the position of Trp382. *J. Am. Chem. Soc. 131*, 4795–4807.
55. Schwede, T., Kopp, J., Guex, N., and Peitsch, M. C. (2003) SWISS-MODEL: an automated protein homology-modeling server. *Nucleic Acids Res. 31*, 3381–3385.
56. Borucki, B., Otto, H., Joshi, C. P., Gasperi, C., Cusanovich, M. A., Devanathan, S., Tollin, G., and Heyn, M. P. (2003) pH dependence of the photocycle kinetics of the E46Q mutant of photoactive yellow protein: protonation equilibrium between I1 and I2 intermediates, chromophore deprotonation by hydroxyl uptake, and protonation relaxation of the dark state. *Biochemistry 42*, 8780–8790.
57. Hendriks, J., van Stokkum, I. H. M., and Hellingwerf, K. J. (2003) Deuterium isotope effects in the photocycle transitions of the photoactive yellow protein. *Biophys. J. 84*, 1180–1191.
58. Novoderezhkin, V. I., Yakovlev, A. G., vanGrondelle, R., and Shuvalov, V. A. (2004) Coherent nuclear and electronic dynamics in primary charge separation in photosynthetic reaction centers: a Redfield theory approach. *J. Phys. Chem. B 108*, 7445–7457.
59. Shuvalov, V. A., and Yakovlev, A. G. (2003) Coupling of nuclear wavepacket motion and charge separation in bacterial reaction centers. *FEBS Lett. 540*, 26–34.
60. Solar, S., Getoff, N., Surdhar, P. S., Armstrong, D. A., and Singh, A. (1991) Oxidation of tryptophan and N-methylindole by $N_3^{\bullet}$, Br^{2-}, and $(Scn)^{2-}$ radicals in light-water and heavy-water solutions—a pulse-radiolysis study. *J. Phys. Chem. 95*, 3639–3643.